Chinese Chemical Letters 36 (2025) 109901

Contents lists available at ScienceDirect

Chinese Chemical Letters

journal homepage: www.elsevier.com/locate/cclet

Anchoring thiol-rich traps in 1D channel wall of metal-organic framework for efficient removal of mercury ions

Xudong Zhao[a], Yuxuan Wang[a], Xinxin Gao[a], Xinli Gao[b,*], Meihua Wang[b], Hongliang Huang[d,*], Baosheng Liu[c]

[a] College of Chemical Engineering and Technology, Taiyuan University of Science and Technology, Taiyuan 030024, China
[b] Instrumental Analysis Center, Taiyuan University of Science and Technology, Taiyuan 030024, China
[c] College of Materials Science and Engineering, Taiyuan University of Science and Technology, Taiyuan 030024, China
[d] State Key Laboratory of Separation Membranes and Membrane Processes, School of Chemical Engineering and Technology, Tiangong University, Tianjin 300387, China

ARTICLE INFO

Article history:
Received 3 January 2024
Revised 21 March 2024
Accepted 16 April 2024
Available online 16 April 2024

Keywords:
Metal-organic frameworks
Thiol groups
Mercury ion
Adsorption
Waste water treatment

ABSTRACT

Metal-organic frameworks (MOFs) attract broad interests in mercury (Hg) ion adsorption field, while unreasonable distribution of active groups commonly restricts their utilization efficiency. In this work, we constructed a new MOF (TYUST-6) with dense thiol-rich traps in the 1D pore wall. This accessible channel and rational distribution of thiols allow the smooth diffusion of Hg ions and thereby result in a high Langmuir adsorption capacity of 1347.6 mg/g, almost reaching the theoretical maximum (1444.3 mg/g). Adsorption equilibrium needs 10 and 30 min at the initial concentrations of 10 and 100 mg/L, respectively. Common co-existing ions and solution pH show almost negligible interferences on the adsorption, and adsorbent regeneration can be well achieved. Combining experimental characterizations and theoretical calculations, the thiol groups in the pore wall are proved to be the dominant interaction sites. Thus, this work reports a novel high-capacity adsorbent for Hg^{2+}, and proposes a feasible guideline for designing effective adsorbents.

Mercury (Hg) pollution problem has become a persistent concern, along with rapid development of industries such as electroplate, chlorine alkali, pharmaceuticals, and battery manufacturing [1]. Due to its persistence, bioaccumulation, and high toxicity, Hg is broadly considered as one of the most hazardous metal elements. Excessive Hg content in water media can induce severe threatens towards human health and environment safety [2]. Thus, it is urgent to effectively eliminate Hg from polluted wastewaters, based on rational treatment methods.

Past decades have witnessed several methods for Hg ions removal, for instance, precipitation, membrane separation, ion exchange, and adsorption [3–5]. Therein, adsorption shows the advantages of simple operation, high selectivity, and excellent applicability for low- or ultra-low-concentration pollutants, if adsorbents are rationally designed. Some traditional porous materials (*e.g.*, carbons, zeolites, and natural minerals [6–8]) show low costs, while still face drawbacks in adsorption capacity or selectivity. Meanwhile, the relatively poorer designability may limit their further improvement for adsorption performances.

Metal-organic frameworks (MOFs) assembled by metal clusters and organic ligands have shown promising applications in adsorption and separation [9–11]. Upon introduction of specific active sites, MOFs will own strong affinity towards targeted ions or molecules [12,13]. Since 2009 [14], some MOFs have been reported for Hg(II) ion removal, among which thiol-decorated samples (*e.g.*, Cu-BTC, MIL-101, UiO-66, MOF-808, and Zr-MSA) play important roles [15–18]. To achieve effective adsorption of Hg(II) ions, one general route is to introduce highly dense active groups such as thiols. However, excessive thiol groups may result in a crowded channel and thereby low use efficiency for these groups. As a result, it often happens that the experimental adsorption capacity is far away from the theoretical maximum.

In this work, to balance the channel permeability and group density, we successfully constructed -SH-rich adsorption traps in the pore wall of a new aluminum-based MOF. As presented in Schemes 1a and b, a self-assembly reaction of chained AlO_6 cluster and dimercaptosuccinic acid (H_2DMSA) results in the Al-DMSA (TYUST-6, TYUST refers to the abbreviation of Taiyuan University of Science and Technology). This Al-based MOF shows an accessible

* Corresponding authors.
E-mail addresses: gaoxinli@tyust.edu.cn (X. Gao), huanghongliang@tiangong.edu.cn (H. Huang).

https://doi.org/10.1016/j.cclet.2024.109901
1001-8417/

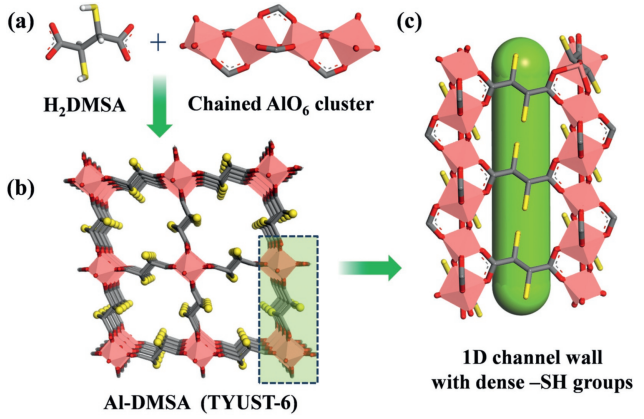

Scheme 1. (a) Organic linker and chained AlO_6 cluster of TYUST-6. (b) Overall framework topology structure of TYUST-6. (c) 1D channel and -SH distribution mode on the channel wall (color: Al, light red; O, red; C, grey; S, yellow; H was omitted for clarity).

one-dimension (1D) channel, on whose walls rich -SH groups are uniformly distributed (Scheme 1c). This structural superiority facilitates the diffusion of Hg(II) ions and the sufficient consumption of -SH groups. On this basis, a high Langmuir adsorption capacity of 1347.6 mg/g was achieved. The detailed adsorption regions and interaction mode were also investigated and discussed.

The unit cell parameters (Table S1 in Supporting information) of TYUST-6 were obtained by indexing the powder X-ray diffraction (XRD) patterns. The preliminary structure was constructed based on the A520 MOF whose organic linker is fumaric acid [19], and then the crystal structure was optimized by periodic density functional theory (DFT) calculations. TYUST-6 crystallizes in the monoclinic crystal system of the P21/C space group. Two adjacent Al polyhedrals share one axial hydroxyl group (H is omitted) to produce an AlO_6 chain. Every two adjacent AlO_6 chains are then connected with DMSA dicarboxylates to result in open 1D channel with a theoretical diameter of ~6.0 Å. Each 1D channel is divided by four walls of DMSA units and four AlO_6 chains. The formula of solvent-free TYUST-6 can be roughly determined as Al(OH)(DMSA).

The experimental XRD patterns are almost consistent with the simulated ones (Fig. 1a). The N_2 adsorption-desorption isotherms show the type-IV curve (Fig. 1b) and the hysteresis loop suggests the presence of mesopore. The pore size distribution curve shows the appearance of a micropore of $d = 1.2$ nm and a mesopore of $d = 7.5$ nm (Fig. S1 in Supporting information), which are larger than the theoretical pore size. This is possibly caused by two factors: (i) MOF particles accumulation; (ii) formation of defective units or missing DMSA linkers (S content: 28.5 wt% in theory, 22.89 wt% in experiment). The Brunauer-Emmett-Teller (BET) specific surface area and pore volume of TYUST-6 were determined to be 264.2 m^2/g and 0.48 cm^3/g, respectively. In the Fourier transform infrared (FTIR) spectrum (Fig. S2 in Supporting information), the dual peaks at 1619 and 1435 cm^{-1} attributed to OCO-Al bonds suggest the coordination of Al ions and DMSA linkers. The peak at 502 cm^{-1} is assigned to Al-O(H)-Al bond. The presence of -SH is confirmed by the weak FTIR peak at 2550 cm^{-1} and S 2p XPS peaks at 165.03 and 163.87 eV (Fig. 1c) [20]. The -SH density of TYUST-6 is quantified to be 7.2 mmol/g, based on organic element analysis (CHNS channel). Benefiting from the high linker density and short linker length, the -SH content of TYUST-6 is higher than that of many reported thiol-MOFs [16,18,21-27], including those consisting of the linkers with dual -SH groups (*e.g.*, MOF-808-DMSA, CAU-1–2SH, Zr-DMSA, and UiO-66–2SH) (Fig. 1d). The scanning electron microscope (SEM) images (Fig. S3 in Supporting information) show the irregular blocky-shaped particles with a homogenous size of ~80 nm. Based on the thermo gravimetric analysis curve (Fig. S4 in Supporting information), the thermal stable temperature is approximately 250 °C.

Based on this distinct framework structure and rich -SH groups, it is expected that TYUST-6 will show promising adsorption for Hg^{2+} ions. From the adsorption isotherm (Fig. 2a), the maximum adsorption amount is 1030 mg/g at the given concentration range (C_0, 10–1000 mg/L). The Langmuir isotherm model was found to better describe the adsorption behaviour than the Freundlich model (Fig. S5 and Table S2 in Supporting information), indicating the monolayer adsorption mode of Hg^{2+} ions onto TYUST-6. It is surprising that the Langmuir adsorption capacity reaches 1347.6 mg/g, almost consistent to the theoretical maximum (1444.3 mg/g) (if one -SH group binds to one Hg^{2+} ion). The adsorption equilibrium at the concentrations of 10 and 100 mg/L needs approximately 10 and 30 min, respectively (Fig. 2b). During a common adsorption process, guest ions are considered to firstly diffuse from solution to adsorbent surface, and subsequently diffuse to interior channels. For the low-concentration Hg^{2+} ions (10 mg/L), the adsorption sites on the surface may be sufficient.

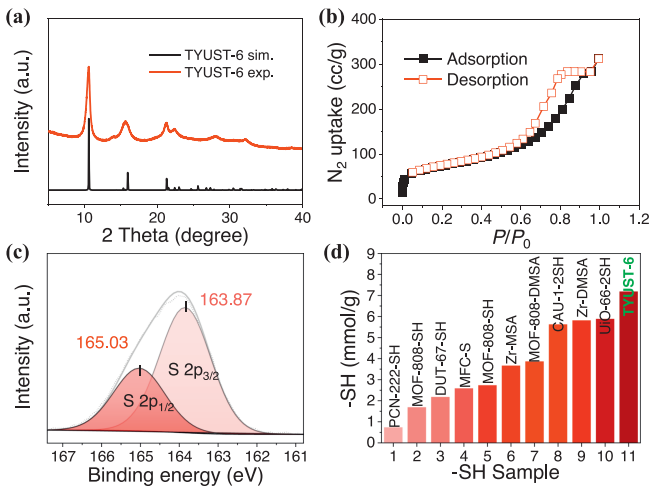

Fig. 1. (a) Simulated and powder XRD patterns. (b) Nitrogen adsorption-desorption curves at 77 K. (c) High-resolution S 2p XPS pattern. (d) -SH content in various reported MOFs (note: the value of UiO-66–2SH is calculated based on perfect crystal).

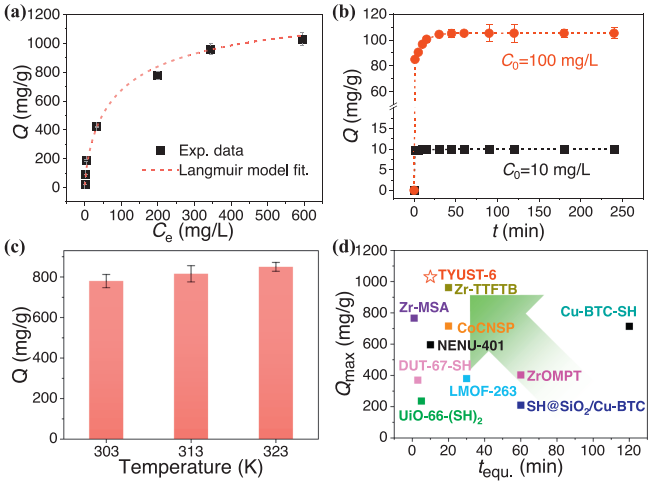

Fig. 2. (a) Adsorption isotherm at 303 K and the Langmuir isotherm model fitting curve (condition: *t*, 12 h; pH, 5.0 ± 0.2; dosage, 0.5 g/L). (b) Adsorption kinetic curves at the initial concentrations of 10 and 100 mg/L (condition: pH, 5.0 ± 0.2; dosage, 0.5 g/L; *T*, 303 K). (c) Adsorption amount at 303–323 K (condition: C_0, 500 mg/L; pH, 5.0 ± 0.2; dosage, 0.5 g/L; *t*, 12 h). (d) Summary of the largest adsorption amount and equilibrium time for various adsorbents.

As a comparison, the adsorption of high-concentration Hg^{2+} ions (100 mg/L) may require an additional pore diffusion process. In general, the diffusion speed in the first step (surface diffusion) is rather faster than that in the second step (pore diffusion) [28,29]. Besides, the adsorption data is well described by the classical *pseudo*-second-order model (Fig. S6 and Table S3 in Supporting information). The effect of temperature on the adsorption was also investigated. It is found that higher temperature benefits to the adsorption (Fig. 2c). A linear fitting between $\ln(Q_e/C_e)$ and $1/T$ was performed (Fig. S7 in Supporting information) and the obtained thermodynamic parameters are listed in Table S4 (Supporting information). The Gibbs free energy change values are all negative at 303–323 K, indicating that Hg^{2+} ion adsorption is spontaneous; the increased values (absolute values) along with the increasing temperature suggest that higher temperature benefits to the adsorption. Besides, the increased entropy value is attributed to the falling off of the hydrated water molecules from hydrated Hg^{2+} ion during the adsorption process.

Furthermore, a comparison with other reported MOF-based adsorbents [15-17,30-36] was carried out. It is clear that TYUST-6 shows superiority considering adsorption capacity and adsorption speed simultaneously (Fig. 2d and Table S5 in Supporting information). Among the other MOFs, UiO-66–2SH also owns a higher -SH content; however, in its cage-window structure, the narrow triangular window is the unique channel for entering the interior pores. This will severely limit the diffusion of guest Hg^{2+} ions, compared with the smooth diffusion in the 1D channel of TYSUT-6. Zr-MSA, DUT-67 and Cu-BTC-SH show lower adsorption amounts, mainly attributed to their less -SH contents. The excellent adsorption in Zr-TTFTB is attributed to the strong affinity of disulfide sites and large diffusion channels. Therefore, based on the comparison above, we suggest this excellent adsorption of TYUST-6 is attributed to the accessible 1D channel structure and high density of active groups.

The effects of some other parameters were investigated. For the concentration of 100 mg/L, the adsorbent dosage of 0.5 g/L can lead to a high removal ratio of 99.3%; with a more dosage of 2.0 g/L, the removal ratio increases to be 99.9% (Fig. 3a). Considering the adsorbent cost, the dosage of 0.5 g/L may be an optimal selection. The effect of pH was investigated under an acidic range because alkaline conditions may result in Hg ion precipitation. It is found that TYUST-6 remains a high removal ratio under a wide range of 2.0–7.0 (Fig. 3b). Solution pH is generally decreased after Hg^{2+} ions adsorption (Fig. S8 in Supporting information), indicating the release of H^+ ions from the -SH groups. In other words, an ion-exchange process between Hg^{2+} and H^+ ions may happen. Actual wastewater commonly contains some other metal ions, which may cause disturbance on Hg^{2+} ion adsorption. As presented in Fig. 3c, in a 9-component solution, Hg^{2+} ion can be still removed almost completely while other 8 classes of metal ions are hardly adsorbed. The K_d value of Hg^{2+} reaches up to 2.2×10^5 mL/g and that of other metal ions are all less than 100 mL/g (Fig. S9 in Supporting information). This huge difference indicates the high selectivity. According to the Hard-Soft Acids and Bases theory by R.G. Pearson [37], thiol group is considered as a class of soft alkaline, which owns stronger affinity towards those soft acids (*e.g.*, Hg^{2+}) and much weaker interaction with borderline acids (*e.g.*, Co^{2+}, Cu^{2+}, and Zn^{2+}) or hard acids (*e.g.*, Li^+, Na^+, K^+, Al^{3+}, and Eu^{3+}). Furthermore, the recyclable use of TYUST-6 was investigated based on a simple solvent elution method. Herein, an ethylenediamine tetraacetic acid disodium (EDTA-2Na, 0.1 mol/L) solution was applied as the eluent to wash out the adsorbed Hg^{2+} ions. After three adsorption-desorption cycles, this adsorbent still has a high removal ratio of 92.1% (Fig. 3d). Besides, TYUST-6 can remain its framework integrality after Hg^{2+} ions adsorption and regeneration treatment (Fig. S10 in Supporting information). These results indicate that TYUST-6 can serve as a potential adsorbent for Hg^{2+} ions in actual wastewater.

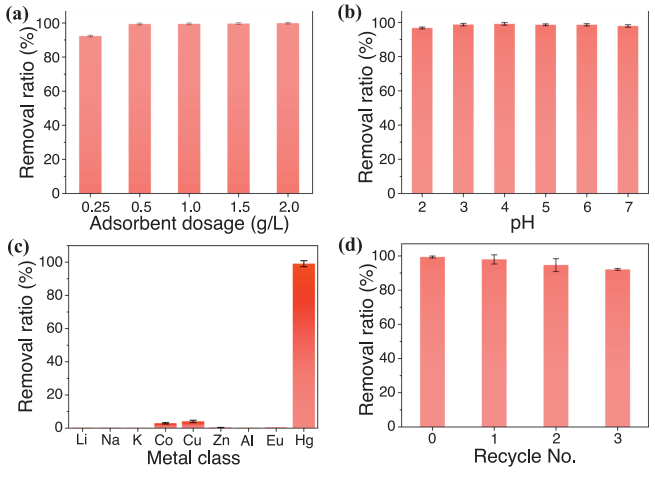

Fig. 3. (a) Removal ratio of Hg^{2+} ion under different adsorbent dosage (condition: C_0, 100 mg/L; *t*, 12 h; pH, 5.0 ± 0.2; *T*, 303 K). (b) Removal ratio of Hg^{2+} ion at pH 2.0–7.0 (condition: C_0, 100 mg/L; *t*, 12 h; dosage, 0.5 g/L; *T*, 303 K). (c) Removal ratios of various metal ions in a nine-component solution (condition: C_0 for all the metal ions, 100 mg/L; *t*, 12 h; dosage, 0.5 g/L; *T*, 303 K). (d) Removal performance of regenerated adsorbent (adsorption condition: C_0, 100 mg/L; *t*, 12 h; dosage, 0.5 g/L; *T*, 303 K).

The adsorption mechanism was investigated firstly based on experimental characterizations. According to the full-survey XPS patterns (Fig. S11 in Supporting information), the presence of Hg^{2+} ions in TYUST-6 is confirmed. The Hg $4f_{7/2}$ peak locates at 100.9 eV (Fig. S12 in Supporting information), close to the 100.8 eV and 101.1 eV of HgS compounds in Wang *et al.*'s work [38] and XPS handbook [20], respectively. This good consistency indicates the formation of Hg-S bonds. In the S 2p pattern (Fig. S13 in Supporting information), the XPS peak of C-SH bond is largely weakened and a new peak for S-Hg bond is formed. An additional proof for the S-Hg interaction was from the weakened FTIR peak of -SH groups after Hg^{2+} adsorption (Fig. S14 in Supporting information). Besides the contribution from -SH groups, the μ-O site also plays a positive effect on the adsorption. From the FTIR spectra, the adsorption of Hg^{2+} ions induces the decrease of μ-O peak at 646 cm^{-1} and the appearance of a new peak at 620 cm^{-1}, possibly attributed to O–Hg bonds. Furthermore, the almost unchanged IR peaks of OCO-Al bonds indicate the high framework stability, consistent to the powder XRD pattern result.

The detailed adsorption mode of Hg^{2+} ions was investigated *via* DFT calculations. TYUST-6 contains three possible classes of -SH-based adsorption sites (Fig. 4): site I: the two diagonal -SH groups in the 1D channel; site II: the two adjacent -SH groups in the 1D channel; site III: the two -SH groups on the 1D pore wall. In site I, the lengths of two S-Hg bonds are 2.398 and 2.396 Å (Fig. 4a) and an obvious electron transfer from S atoms to Hg atom happens (Fig. 4b). As a result, the binding energy in site I is −52.2 kcal/mol. Still in the same structural plane, the binding energy in site II is increased to −129.2 kcal/mol, due to the relatively shorter S-S distance (Fig. 4c). The two bridged O atoms seem likely to participate in the adsorption, while so far O–Hg atoms distances indicate the weak interactions. The charge difference calculation also illustrates the absence of the contribution of the O atoms (Fig. 4d). In site III, Hg atom is simultaneously interacted with two S atoms and two bridged O atoms (Fig. 4e). The other one visual angel was provided for clearer observation (Fig. S15 in Supporting information). The shorter atoms distance induces a stronger adsorption driven force with a binding energy of −172.1 kcal/mol. The charge density difference image in Fig. 4f also confirms the synergic contribution

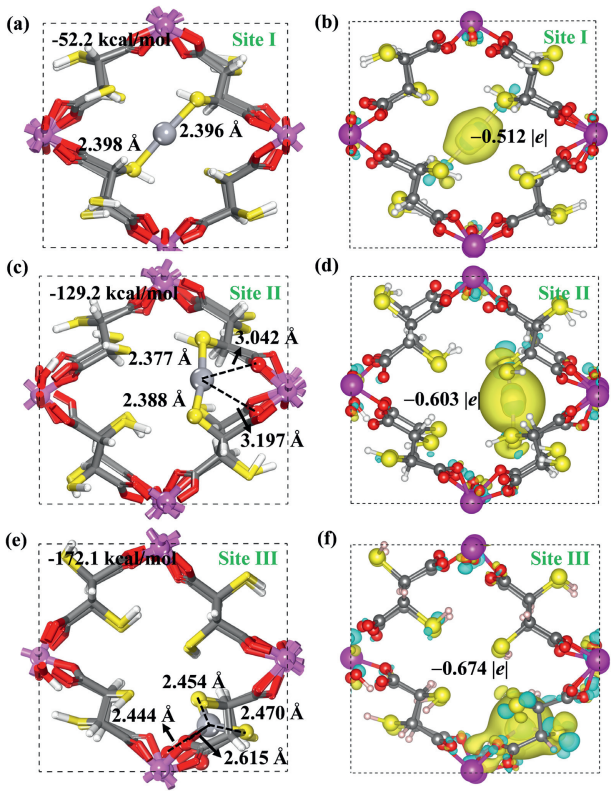

Fig. 4. DFT-calculated configurations of Hg^{2+} adsorption in adsorption site I (a), site II (c) and site III (e). Isosurfaces (level 0.01) of charge density differences of TYUST-6 with Hg^{2+}: site I (b), site II (d) and site III (f). Yellow indicates electron accumulation, and light blue indicates depletion. The minus sign indicates electron accumulation. Color: Al, pink; Hg, silver; O, red; C, grey; S, yellow; H, white.

of two S atoms and two O atoms. In addition, the transferred electron number from the active groups to Hg^{2+} ion follows the order: Site III (0.674e) > Site II (0.603e) > Site I (0.512e). Thus, from the viewpoint of adsorption thermodynamic, Hg ions may be easier adsorbed in site III. Benefiting from this, Hg ions will be captured in the pore wall and thereby will not block the 1D channel, superior to the adsorption modes in site I and II.

In summary, a novel TYUST-6 adsorbent with rich thiol groups was explored for effective Hg^{2+} ions adsorption. Benefiting from the accessible 1D channel, the thiol sites on the pore wall can be utilized sufficiently. On this basis, TYUST-6 exhibits a high Langmuir adsorption amount of 1347.6 mg/g and short adsorption equilibrium time (10–30 min), which is superior to most of reported MOF-based adsorbents. Higher temperature is found to promote the adsorption and this adsorbent can be well regenerated. Solution pH and co-existing metal ions have negligible effects, under the low concentration of 100 mg/L. Our work highlights the synergic importance of 1D channel and dense ion traps on Hg^{2+} ions adsorption. We expect this work will provide a guideline for designing efficient MOFs adsorbents in the future.

Declaration of competing interest

The authors declare that they have no known competing financial interests or personal relationships that could have appeared to influence the work reported in this paper.

CRediT authorship contribution statement

Xudong Zhao: Investigation, Writing – original draft, Methodology. **Yuxuan Wang:** Investigation, Methodology. **Xinxin Gao:** Investigation, Methodology. **Xinli Gao:** Conceptualization, Writing – review & editing. **Meihua Wang:** Investigation. **Hongliang Huang:** Supervision, Writing – review & editing. **Baosheng Liu:** Supervision, Writing – review & editing.

Acknowledgments

This work was supported by the National Natural Science Foundation of China (No. 22208230) and Fundamental Research Program of Shanxi Province (No. 202103021223281).

Supplementary materials

Supplementary material associated with this article can be found, in the online version, at doi:10.1016/j.cclet.2024.109901.

References

[1] R. Melamed, A. Benvindo da Luz, Sci. Total Environ. 368 (2006) 403–406.
[2] C.A.R. Hernández, M.R.V. Pérez, I.R. Soto, et al., Chemosphere 311 (2023) 136965.
[3] O.R. Marinho, M.Y. Kamogawa, J.R. Ferreira, B.F. Reis, Microchem. J. 156 (2020) 104978.
[4] M. Zunita, Membranes 11 (2021) 269.
[5] C. Yang, J. Tian, F. Jiang, Chem. Rec. 21 (2021) 1–19.
[6] C.J. Hsu, Y.Z. Xiao, H.C. His, Chemosphere 263 (2021) 127966.
[7] G.K.R. Angaru, L.P. Lingamdinne, Y.L. Choi, et al., Mater. Today Chem. 22 (2021) 100577.
[8] M. Monier, D.A. Abdel-Latif, J. Hazard. Mater. 209-210 (2012) 240–249.
[9] Y.F. Zhang, Z.H. Zhang, H. Fang, et al., Inorg. Chem. 62 (2023) 20513–20519.
[10] J. Zhong, J. Zhou, M. Xiao, et al., Chin. Chem. Lett. 33 (2022) 973–978.
[11] C. Wang, X. Liu, T. Yang, et al., Sep. Purif. Technol. 320 (2023) 124144.
[12] Y. Shu, Y. Chen, Q. Han, et al., ACS EST Eng. 3 (2023) 1042–1052.
[13] X. Gao, R. Ding, H. Huang, B. Liu, X. Zhao, Chem. Commun. 59 (2023) 13183–13186.
[14] X.P. Zhou, Z. Xu, M. Zeller, A.D. Hunter, Chem. Commun. (2009) 5439–5441.
[15] X. Gao, B. Liu, X. Zhao, Chemosphere 317 (2023) 137891.
[16] X. Zhao, X. Gao, Y.N. Zhang, et al., J. Colloid Interface Sci. 631 (2023) 191–201.
[17] F. Ke, L.G. Qiu, Y.P. Yuan, et al., J. Hazard. Mater. 196 (2011) 36–43.
[18] L. Huang, M. He, B. Chen, B. Hu, J. Mater. Chem. A 4 (2016) 5159–5166.
[19] E. Alvarez, N. Guillou, C. Martineau, et al., Angew. Chem. Int. Ed. 54 (2015) 3664–3669.
[20] J.F. Moulder, W.F. Stickle, P.E. Sobol, K.D. Bomben, Handbook of X-Ray Photoelectron Spectroscopy, 2nd ed., Perkin-Elmer Corporation, Minnesota, 1992.
[21] X. Zhao, M. Wu, H. Huang, B. Liu, Sep. Purif. Technol. 328 (2024) 125127.
[22] K.K. Yee, N. Reimer, J. Liu, et al., J. Am. Chem. Soc. 135 (2013) 7795–7798.
[23] S. Nazri, M. Khajeh, A.R. Oveisi, et al., Sep. Purif. Technol. 259 (2021) 118197.
[24] P. Yang, Y. Shu, Q. Zhuang, Y. Li, J. Gu, Chem. Commun. 55 (2019) 12972–12975.
[25] X. Zhao, L. Pei, Y.N. Zhang, et al., GreenChE 3 (2022) 405–412.
[26] C. Ji, Y. Ren, H. Yu, et al., Chem. Eng. J. 430 (2022) 132960.
[27] X. Zhao, X. Gao, T. Yang, Z. Liu, B. Liu, Sep. Purif. Technol. 320 (2023) 124062.
[28] H. Guo, F. Lin, J. Chen, F. Li, W. Weng, Appl. Organomet. Chem. 29 (2015) 12–19.
[29] H. Wang, J. Zhang, P. Wang, et al., Chin. Chem. Lett. 31 (2020) 2789–2794.
[30] M.Q. Li, Y.L. Wong, T.S. Lum, et al., J. Mater. Chem. A 6 (2018) 14566–14570.
[31] S.Y. Jiang, W.W. He, S.L. Li, Z.M. Su, Y.Q. Lan, Inorg. Chem. 57 (2018) 6118–6123.
[32] M.R. Sorhrabi, Microchin. Acta 181 (2014) 435–444.
[33] N.D. Rudd, H. Wang, E.M.A. Fuentes-Fernandez, et al., ACS Appl. Mater. Interfaces 8 (2016) 30294–30303.
[34] K. Leus, J.P.H. Perez, K. Folens, et al., Faraday Discuss. 201 (2017) 145–161.
[35] Y. Tang, M. Zheng, W. Xue, H. Huang, G. Zhang, Sep. Purif. Technol. 287 (2022) 120577.
[36] J. Li, Q. Duan, Z. Wu, et al., Chem. Eng. J. 383 (2020) 123189.
[37] R.G. Pearson, J. Am. Chem. Soc. 85 (1963) 3533–3539.
[38] H. Wang, J.J. Zhu, Ultrason. Sonochem. 11 (2004) 293–300.